JOURNAL OF SOLID STATE CHEMISTRY **123,** 21–29 (1996)
ARTICLE NO. 0147

Synthesis, Crystal Structure, and Physical Properties of a New Reduced Lanthanum Niobium Oxide: $LaNb_7O_{12}$

J. Xu, T. Emge, and M. Greenblatt[1]

Department of Chemistry, Rutgers, The State University of New Jersey, Piscataway, New Jersey 08855-0939

Received September 5, 1995; accepted December 20, 1995

Single crystals of $LaNb_7O_{12}$ were obtained by annealing a mixture of La_2O_3, Nb_2O_5, and Nb in 1:1:1 molar ratio with NH_4Cl in a sealed quartz tube. $LaNb_7O_{12}$ crystallizes in the monoclinic space group $P2_1/c$ with cell parameters a = 10.762(1), b = 9.192(1), c = 10.314(1) Å, β = 104.25°, and z = 4 formula units per cell. The structure was determined from single-crystal X-ray diffraction data and refined to a residual of $R(F) = 0.037$ and $R_w(F^2) = 0.077$ for 119 variable parameters and a unique data set of 1400 observations [$I > 2\sigma(I)$]. The essential building units of the structure are Nb_6 and NbO_6 octahedra and La ions in eight coordination of oxygen. Two NbO_6 octahedra corner-share to form a pair and connect with Nb_6 octahedra via oxygen atoms. Nb_6 octahedra share both apical and inner oxygen atoms with neighboring Nb_6 to form columns of Nb_6O_{12} clusters along the c axis. The Nb_6O_{12} clusters exhibit 14 valence electrons in M–M bonding states. $LaNb_7O_{12}$ is a semiconductor with an activation energy of 0.08 eV. The magnetic susceptibility data show weak temperature-independent paramagnetism. The Madelung part of the lattice energy has been calculated and is discussed.

INTRODUCTION

Many reduced molybdenum chalcogenides and oxomolybdates with structures built up of condensed Mo_6 octahedra are well known (1). The condensation, which occurs along edges or faces of the Mo_6 octahedra, leads to a variety of oligomeric and infinite cluster structures. Because of the low-dimensional (LD) structural and electronic properties of these materials, the physical properties, especially electronic instabilities associated with LD structures, are of interest. Although a few oxomolybdates with discrete Mo_6 octahedra are known (2), in the corresponding oxoniobates both discrete (e.g., $Ba_3Nb_{21-x}Si_2O_{14}$ (3), $Mg_3Nb_6O_{11}$ (4), Na(Si, Nb)$Nb_{10}O_{19}$ (5)) and condensed Nb_6O_{12} clusters (e.g., $BaNb_7O_9$ (6), $K_4Al_2Nb_{11}O_{21}$ (7)) have been reported as characteristic building units (8).

The Nb_6 octahedra in the "Nb_6O_{18}" clusters are bonded to oxygen atoms and can be represented by the formula $Nb_6O^i_{12}O^a_6$. There are twelve so-called inner oxygen atoms (O^i) above the edges of a Nb_6 octahedron and six oxygens above the apices of the octahedron that are designated as outer ligands (O^a) (Fig. 1). By convention, the O^a ligands are not included when discussing the discrete cluster, and it is referred to as a Nb_6O_{12}, rather than a Nb_6O_{18} cluster; this convention will be followed in this paper hereafter. The discrete Nb_6O_{12} clusters may be connected through bridging oxygen atoms in three different linkages, i.e., O^{i-i}, O^{a-a}, and O^{a-i}. Typically electropositive metal ions A(A = Na, K, Rb, Ba, La, and Eu) donate electrons to the Nb_6O_{12} cluster, and stabilize the structure.

In the ternary La–Nb–O system, only one oxide, $LaNb_8O_{14}$, has been reported so far (9). It should be possible that more reduced niobium oxides with La exist. In our investigations of the ternary La–Nb–O systems, we obtained a new reduced lanthanum niobium oxide containing discrete Nb_6O_{12} clusters with 14 valence electrons: $LaNb_7O_{12}$. We report here the synthesis, single crystal structure determination, and the study of the physical properties of $LaNb_7O_{12}$. A comparison of the structure, as well as the physical properties, with related reduced niobium cluster compounds are also presented.

EXPERIMENTAL

Sample Preparation

The starting materials were Nb (Johnson Matthey Electronics, 99.99%), Nb_2O_5 (Alfa, 99.5%), La_2O_3 (Aldrich, 99.99%), and NH_4Cl (Fisher, ACS grade). Black crystals of $LaNb_7O_{12}$ were prepared by heating a pellet of an intimate mixture of Nb, Nb_2O_5, and La_2O_3 in the molar ratio 1:1:1 and with 5% of NH_4Cl at 1250°C in a sealed quartz tube for 10 days, followed by slow cooling at 5°C/hr to 1100°C, 50°C/hr to 500°C, and then quenching to room temperature. Black plate-like crystals were found embedded in the pellets. The crystals were washed with water before X-ray intensity data collection.

[1] To whom correspondence should be addressed.

0022-4596/96 $18.00

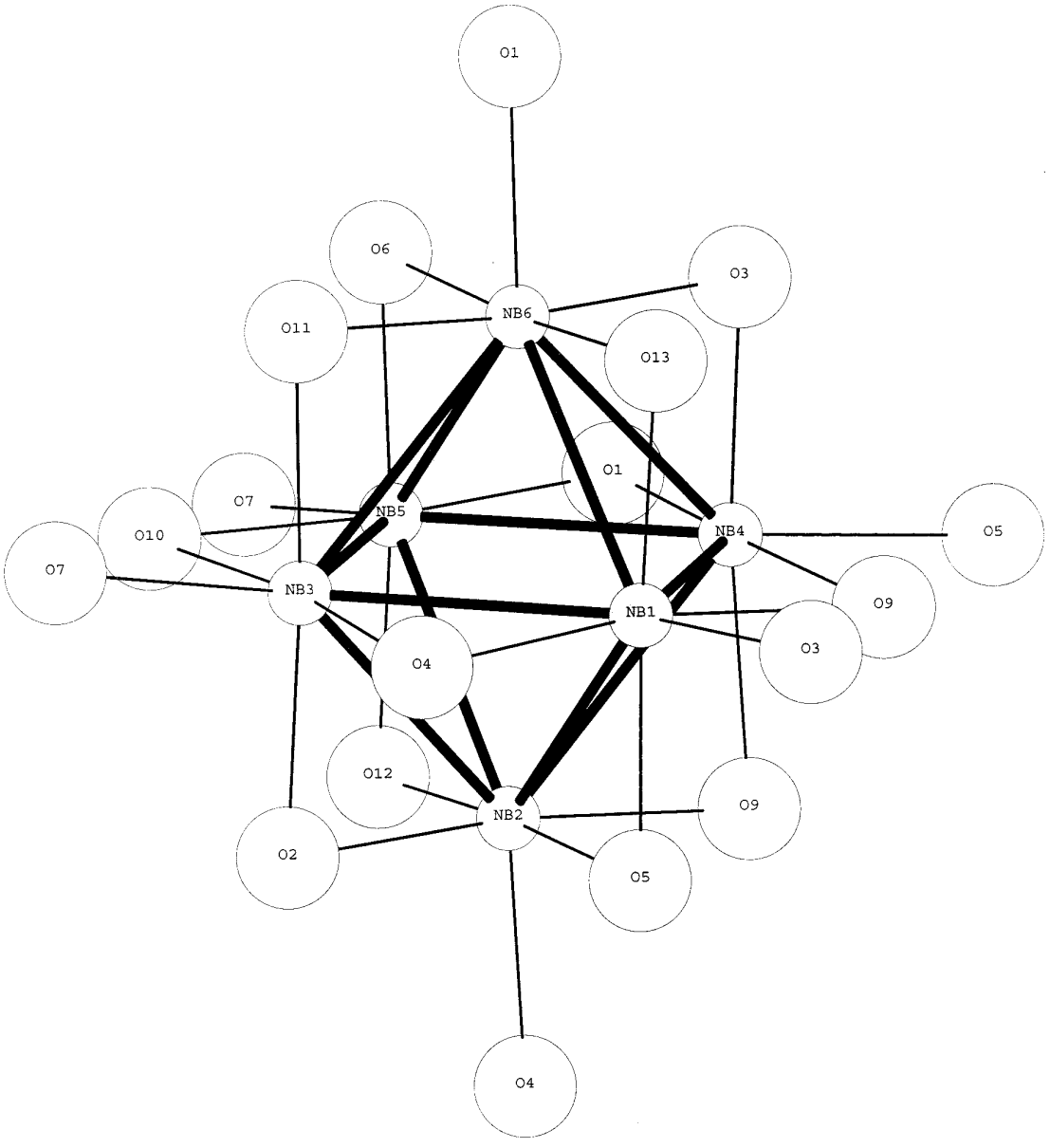

FIG. 1. The $Nb_6O_{12}{}^{i}O_6{}^{a}$ unit occurring in $LaNb_7O_{12}$.

Once the crystal composition had been determined polycrystalline samples of $LaNb_7O_{12}$ were prepared using a stoichiometric mixture of Nb, NbO_2, and La_2O_3. The mixture was thoroughly ground, pelletized, sealed in an evacuated quartz tube, and heated at 1300°C for 2 days.

Single Crystal X-Ray Diffraction Data

A single crystal of $LaNb_7O_{12}$ with dimensions $0.016 \times 0.036 \times 0.044$ mm^3 was selected for X-ray intensity data collection. The data were collected on an Enraf-Nonius CAD4 diffractometer with graphite monochromatized Mo-$K\alpha$ radiation ($\lambda' = 0.71073$ Å) at room temperature. The intensity data were measured up to $\theta = 26°$ with ω scan mode. The unit cell parameters and orientation matrix for data collection were determined by the least-squares fitting of 25 reflections with $32° < 2\theta < 46°$. Of the 2277 reflections collected in the $\pm h$, $\pm k$, $+l$ quadrant, 1400 had $I > 2\sigma(I)$. The intensity of three standard reflections varied less than 1% during the data collection. The data were corrected for Lorentz effects and polarization. A numerical (SHELX76) absorption correction was performed, and the transmission factors were in the range 0.606–0.823. The cell parameters and details of the data

TABLE 1
Summary of Crystal Data and Structure Refinement Results for $LaNb_7O_{12}$

Crystal data	
Formula	$LaNb_7O_{12}$
Space group	$P2_1/c$
Cell dimensions	a = 10.762(1) Å b = 9.192(1) Å c = 10.314 (1) Å β = 104.25(1)°
Volume (Å^3)	988.9(2)
Z	4
λ (Mo$K\alpha$) (Å)	0.71073
Scan mode	ω
Total data collected	2277
Max 2θ (°)	52
Standard reflections	3 measured every 7200 s
Reflection with $I > 2\sigma(I)$	1400
μ (cm^{-1})	121
Solution and refinement	
Data/parameters/restraints	1916/119/42
Agreement factors ($I > 2\sigma(I)$)[a]	$R_{(F)} = 0.037$ $R_{w(F^2)} = 0.077$
Agreement factors (all data)[a]	$R_{(F)} = 0.069$ $R_{w(F^2)} = 0.086$
Goodness-of-fit on all F^2[b]	1.07
Residual peaks (e/Å^3)	−2.3, 2.4

[a] $R_{(F)} = \Sigma||F_o| - |F_c||/\Sigma |F_o|$. $R_{w(F^2)} = \{\Sigma[w(F_o^2 - F_c^2)^2]/\Sigma [w(F_o^2)^2]\}^{1/2}$.
[b] G.O.F. $= \{\Sigma (w(F_o^2 - F_c^2)^2)/(N_{obs} - N_{parm})\}^{1/2}$.

collection are given in Table 1. The U_{ij} components of the La atom displacement parameters were restrained to be isotropic within an estimated standard deviation of 0.01 Å.

Determination and Refinement of the Structure

SHELXS86 and SHELXL93 packages were used for the crystal structure solution and refinement, respectively. The general reflection conditions, $l = 2n$ for $h0l$ and $k = 2n$ for $0k0$, were consistent with space group $P2_1/c$. The La and Nb atom coordinates were found using direct methods and the O atoms were located by Fourier methods to complete the structural model. The structure and thermal parameters refined by full-matrix least-squares methods led to $R(F) = 0.037$ and $R_w(F^2) = 0.077$ for 1400 observed data with $I > 2\sigma(I)$. The maximum and minimum residual electron densities in the final difference Fourier map were 2.4 and −2.3 e/Å^3, respectively, and were near the La atoms. The final positional and equivalent isotropic displacement parameters are given in Table 2. Table 3 gives the final anisotropic displacement parameters for the non-O atoms. Table 4 contains the bond distances and angles for $LaNb_7O_{12}$.

Electrical Resistivity and Magnetic Susceptibility Measurements

Electrical resistivity measurements on a pellet of $LaNb_7O_{12}$ were made by a standard four-probe technique with a Displex Cryostat (APD cryogenics, model DE 202) in the temperature range 150–300 K. Indium leads and silver paint were used to make ohmic contacts to the sample. There was no appreciable variation of the resistivity curve between cooling and heating cycles.

Magnetic susceptibility data on a pellet of $LaNb_7O_{12}$ were recorded with a Quantum Design SQUID magnetometer in the temperature range 2.5 ∼ 300 K. The applied magnetic field was 10,000 G.

DISCUSSION

Synthesis

The plate-like, black single crystals grown in the presence of NH_4Cl were embedded on the surface of the pellet. No crystals were transported. The 5% NH_4Cl presumably served to enhance localized melting, which promoted the formation of the crystals. The synthesis of the corresponding polycrystalline $LaNb_7O_{12}$ sample was attempted from stoichiometric mixtures (e.g., no NH_4Cl) of different starting materials: (i) La_2O_3, Nb, NbO_2; (ii) La_2O_3, NbO, NbO_2; (iii) La_2O_3, Nb, Nb_2O_5. At heating temperatures below 1250°C, significant amounts of the $LaNb_7O_{12}$ phase did not form for any of the preparations. However, good

TABLE 2
Atomic Fractional Coordinates and Equivalent Isotropic Displacement Coefficients (Å^2)[a] for $LaNb_7O_{12}$

Atom	x	y	z	$U_{(equiv)}$
Nb1	0.41905(9)	0.1198(1)	0.1854(1)	0.0035(2)[b]
Nb2	0.28002(9)	0.1170(1)	0.9073(1)	0.0038(2)[b]
Nb3	0.15464(9)	0.1262(1)	0.1175(1)	0.0042(2)[b]
Nb4	0.58750(9)	0.1344(1)	0.9687(1)	0.0039(2)[b]
Nb5	0.14867(8)	−0.1277(1)	−0.03934(9)	0.0031(2)[b]
Nb6	0.71735(9)	0.1244(1)	0.7669(1)	0.0038(2)[b]
Nb7	−0.00054(9)	0.1143(1)	0.3394(1)	0.0041(2)[b]
La	0.33100(6)	0.48464(7)	0.05287(7)	0.0085(2)[b]
O1	0.7190(7)	0.2290(8)	0.5796(8)	0.0061(16)
O2	0.1511(7)	0.2649(8)	−0.0452(8)	0.0078(17)
O3	0.5868(7)	0.2695(8)	0.8123(8)	0.0074(17)
O4	0.2901(7)	0.2310(8)	0.7217(8)	0.0041(16)
O5	0.4233(7)	0.2514(8)	0.0200(8)	0.0032(16)
O6	0.1364(7)	−0.2598(8)	0.1211(8)	0.0043(16)
O7	0.0040(7)	0.2340(8)	0.1863(8)	0.0057(16)
O8	0	0	0.5	0.0124(23)
O9	0.5692(6)	0.0003(8)	0.1379(7)	0.0036(14)
O10	0	0	0	0.0036(20)
O11	0.1514(7)	0.0077(8)	0.2928(7)	0.0046(15)
O12	−0.1395(6)	0.0061(8)	0.2166(7)	0.0058(15)
O13	0.4291(6)	−0.0022(8)	0.3555(7)	0.0060(15)

[a] Estimated standard deviations of refined parameters are enclosed in parentheses.
[b] Atoms are refined anisotropically:
$U_{(equiv)} = \frac{1}{3} (U_{11}a^{*2}a^2 + U_{22}b^{*2}b^2 + U_{33}c^{*2}c^2 + U_{12}a^*b^*ab \cos\gamma + U_{13}a^*c^*ac \cos\beta + U_{23}b^*c^*bc \cos\alpha)$.

TABLE 3
Anosotropic Displacement Parameters (Å^2)[a] for $LaNb_7O_{12}$

Element	U_{11}	U_{22}	U_{33}	U_{23}	U_{13}	U_{12}
Nb1	0.0039(4)	0.0038(5)	0.0035(5)	−0.0004(4)	0.0021(4)	−0.0000(4)
Nb2	0.0044(4)	0.0045(5)	0.0033(5)	0.0006(4)	0.0024(3)	0.0002(4)
Nb3	0.0045(5)	0.0055(5)	0.0035(5)	−0.0000(4)	0.0026(4)	0.0002(4)
Nb4	0.0045(4)	0.0044(5)	0.0038(5)	−0.0000(4)	0.0032(4)	0.0000(4)
Nb5	0.0034(5)	0.0041(5)	0.0026(5)	−0.0006(4)	0.0023(4)	0.0002(4)
Nb6	0.0053(4)	0.0041(5)	0.0031(5)	0.0001(4)	0.0028(4)	−0.0001(4)
Nb7	0.0044(5)	0.0057(5)	0.0031(5)	0.0000(4)	0.0030(4)	−0.0000(4)
La1	0.0109(3)	0.0067(3)	0.0090(3)	0.0003(3)	0.0047(3)	0.0005(3)

Note. The anisotropic displacement exponent takes the form $-2\pi^2[h^2a^{*2}U_{11} + \cdots + 2hka^*b^*U_{12}]$.
[a] Estimated standard deviations are enclosed in parentheses.

TABLE 4
Bond Distances (Å) and Angles (°)
for $LaNb_7O_{12}$

Nb(1)–O(3)	2.201(8)	Nb(2)–O(2)	2.085(8)
Nb(1)–O(4)	2.050(7)	Nb(2)–O(4)	2.208(7)
Nb(1)–O(5)	2.101(7)	Nb(2)–O(5)	2.090(7)
Nb(1)–O(9)	2.108(7)	Nb(2)–O(9)	2.095(7)
Nb(1)–O(13)	2.062(7)	Nb(2)–O(12)	2.062(7)
Nb(1)–Nb(2)	2.890(1)	Nb(2)–Nb(3)	2.823(1)
Nb(1)–Nb(3)	2.759(1)	Nb(2)–Nb(4)	2.848(1)
Nb(1)–Nb(4)	2.816(1)	Nb(2)–Nb(5)	2.783(1)
Nb(1)–Nb(6)	2.791(1)		
		Nb(4)–O(1)	2.023(8)
Nb(3)–O(2)	2.100(8)	Nb(4)–O(3)	2.034(8)
Nb(3)–O(4)	2.057(7)	Nb(4)–O(5)	2.241(7)
Nb(3)–O(7)	2.163(8)	Nb(4)–O(9)$^{\#1}$	2.161(7)
Nb(3)–O(10)	2.143(1)	Nb(4)–O(9)$^{\#2}$	2.185(7)
Nb(3)–O(11)	2.118(7)	Nb(4)–Nb(5)	2.753(1)
Nb(3)–Nb(5)	2.832(1)	Nb(4)–Nb(6)	2.779(1)
Nb(3)–Nb(6)	2.796(1)		
		Nb(6)–O(1)	2.163(8)
Nb(5)–O(1)	2.056(8)	Nb(6)–O(3)	2.073(8)
Nb(5)–O(6)	2.083(8)	Nb(6)–O(6)	2.114(7)
Nb(5)–O(7)	2.174(8)	Nb(6)–O(11)	2.068(7)
Nb(5)–O(10)	2.103(1)	Nb(6)–O(13)	2.088(7)
Nb(5)–O(12)	2.124(7)		
Nb(5)–Nb(6)	2.825(1)		
La–O(1)	2.615(8)	La–O(5)	2.421(7)
La–O(2)	2.808(8)	La–O(11)	2.895(7)
La–O(3)	2.686(8)	La–O(13)$^{\#3}$	2.519(7)
La–O(4)	2.744(8)	La–O(13)$^{\#4}$	2.524(7)

Nb(7)	Distance	Angles				
O(7)	1.935(8)					
O(8)	1.961(1)	177.2(2)				
O(12)	1.974(7)	86.0(3)	96.7(2)			
O(6)	1.984(7)	90.2(3)	89.3(2)	86.9(3)		
O(11)	2.061(7)	84.2(3)	96.0(2)	97.5(3)	172.7(3)	
O(2)	2.088(8)	89.4(3)	87.9(2)	175.1(3)	94.8(3)	80.3(3)
	Nb(7)	O(7)	O(8)	O(12)	O(6)	O(11)

Note. Estimated standard deviations are enclosed in parentheses. $^{\#1}$ $-x + 1, -y, -z + 1$; $^{\#2}x, y, z - 1$; $^{\#3}x, -y + \frac{1}{2}, z - \frac{1}{2}$; $^{\#4}-x + 1$ $y + \frac{1}{2}, -z + \frac{1}{2}$.

yields of polycrystalline $LaNb_7O_{12}$ formed at 1300°C for mixtures (i) and (ii) above. The third mixture (La_2O_3, Nb, Nb_2O_5) resulted in poorly crystalline $LaNb_7O_{12}$. The powder X-ray diffraction (PXD) patterns could be indexed in space group $P2_1/c$ with cell parameters $a = 10.763(4)$, $b = 9.192(2)$, $c = 10.318(2)$ Å, and $\beta = 104.26(2)°$, which are in excellent agreement with the single crystal results (Table 1). The observed and calculated d spacing and the associated relative intensities of the PXD reflections are listed in Table 5.

Description of the Crystal Structure

The basic building units of $LaNb_7O_{12}$ are Nb_6 octahedra, NbO_6 octahedra, and eight-coordinated LaO_8. Nb_6 octahedra connect with oxygen atoms exclusively to give the characteristic clusters of $Nb_6O^i_{12}O^a_6$ (Fig. 1). The Nb_6O_{12} clusters are discrete, rather than condensed. Two NbO_6 octahedra corner share to form Nb_2O_{11} pairs (Fig. 2a). The framework of $LaNb_7O_{12}$ is made up of double columns of discrete $Nb_6O^i_{12}O^a_6$ units, running along the c crystallographic direction, separated by a column of Nb_2O_{11} octahedra pairs along the a axis (Fig. 3). The Nb_6O_{12} clusters are related by a twofold screw axis along the b axis and are interconnected by sharing both their inner (O^i) and apical (O^a) oxygen atoms. The Nb_2O_{11} pairs also share their oxygens with the Nb_6O_{12} clusters. The La ions are located in eight oxygen coordinated interstices of the lattice (Fig. 2b). Figure 4 illustrates the complete structure projected in the bc plane.

Of the seven crystallographically unique niobium atoms, six Nb atoms form the Nb_6 metal octahedron (Fig. 1). The Nb–Nb bond distances within the Nb_6O_{12} clusters are comparable to those observed in other reduced niobium oxides (8). However, the Nb_6 octahedron is significantly distorted, as evidenced in the varied Nb–Nb bond distances (Table 4). In the basal plane of the Nb_6 octahedron, the Nb–Nb distances of opposite edges are 2.753(1) vs 2.759(1) Å and 2.816(1) vs 2.832(1) Å, respectively. Thus the basal plane is more or less rectangular, rather than square

TABLE 5
X-Ray Powder Diffraction Data for $LaNb_7O_{12}$

h	*k*	*l*	*d*-calc.	*d*-obs.	Intensity
0	1	1	6.768	6.778	9
−1	0	2	5.016	5.024	4
0	2	0	4.596	4.605	7
0	2	1	4.176	4.174	7
1	0	2	4.130	4.138	6
−1	2	1	4.022	4.017	7
−2	2	1	3.437	3.436	21
−3	1	1	3.327	3.331	7
2	2	1	3.108	3.101	11
−2	2	2	3.083	3.082	8
−2	1	3	3.012	3.010	12
0	3	1	2.930	2.931	41
3	1	1	2.902	2.901	13
−1	3	1	2.875	2.873	4
1	1	3	2.826	2.829	27
−1	2	3	2.749	2.750	36
−2	3	1	2.637	2.638	9
−1	0	4	2.580	2.580	22
3	2	1	2.547	2.550	5
−1	1	4	2.484	2.483	60
−4	2	1	2.322	2.321	4
0	4	0	2.298	2.297	14
−3	1	4	2.248	2.249	25
−5	1	1	2.094	2.094	6
0	4	2	2.088	2.088	6
1	2	4	2.061	2.062	6
1	4	2	2.008	2.009	7
−1	3	4	1.973	1.973	100
3	2	3	1.952	1.950	7
−3	4	2	1.877	1.878	8
0	5	1	1.808	1.808	14
−1	5	1	1.795	1.795	13
−2	5	1	1.732	1.732	7
−1	4	4	1.716	1.716	42
−5	1	5	1.636	1.636	23
−1	5	4	1.497	1.497	36
3	2	5	1.489	1.489	22

shaped. The average bond distance between the four basal Nb atoms and Nb(6) is slightly shorter (~2.798 Å) than that between Nb(2) (~2.836 Å). Thus it appears that half of the Nb_6 octahedron is elongated. The bond distances between the Nb and O^a and O^i atoms are expected to be in the range from 2.15 ~ 2.35 Å and from 2.02 to 2.13 Å (5), respectively. In $LaNb_7O_{12}$, the Nb–O^a distances (2.16 to 2.24 Å) are within the expected range; the Nb–O^i distances also fall into the expected range, except for two longer ones, Nb(4)–$O^i(9)^{\#1}$ (2.161(7) Å) and Nb(4)–$O^i(9)^{\#2}$(2.185(7) Å) (Table 4). These two longer bond distances are attributed to the distortion of Nb_6 octahedron in which the Nb–Nb bond distances within the Nb(1)–Nb(2)–Nb(4) triangular plane are longer than the rest of the Nb–Nb bond distances.

The Nb(7) atoms form the centers of the NbO_6 octahedra in the dimers (Fig. 2a). The Nb–O bond distances (1.94 to 2.09 Å) in these NbO_6 are normal for niobium with octahedral coordination to oxygen. However, some of the bond angles of O–Nb–O deviate from 90° by up to 9° (Table 4), which indicates that the NbO_6 octahedra are strongly distorted.

The La atoms are coordinated to eight oxygen atoms (Fig. 2b). The La–O bond distances are in the range from 2.42 to 2.90 Å; the latter are much longer than those in lanthanum haloniobates (10, 11) with the same coordination. This might arise from the larger Coulombic repulsion between divalent anions (O^{2-}) than that between O^{2-} and Cl^-.

Bond-Order Sum

Bond-order sums (12) were calculated using

$$s = \exp[(r_0 - r)/B],$$

where $B = 0.37$ and r_0(Nb–O) = 1.912. The bond-order sum for the Nb(7) atom which is octahedrally coordinated to oxygen atoms is 4.77. Therefore, the 5+ oxidation state is assigned for Nb(7). The La ion is assumed to have oxidation state 3+. Accordingly, in $La^{3+}Nb^{5+}(7)Nb_6O_{12}^{2-}$, there are $24 - 3 - 5 = 16$ negative charges to be compensated by the six niobium cluster atoms. Thus, there are 14 electrons remaining in metal–metal bonding states per Nb_6 cluster, a feature which is also found in $M_3Nb_6O_{11}$ (M = Mg or Mn) (4) and MNb_8O_{14}(M = Sr, Ba) (13, 14).

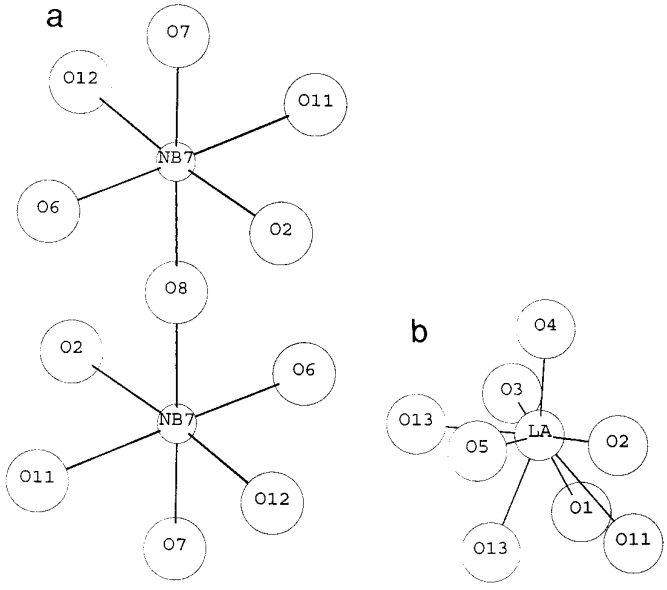

FIG. 2. (a) Corner-sharing of two NbO_6 octahedra. (b) Lanthanum coordination in $LaNb_7O_{12}$.

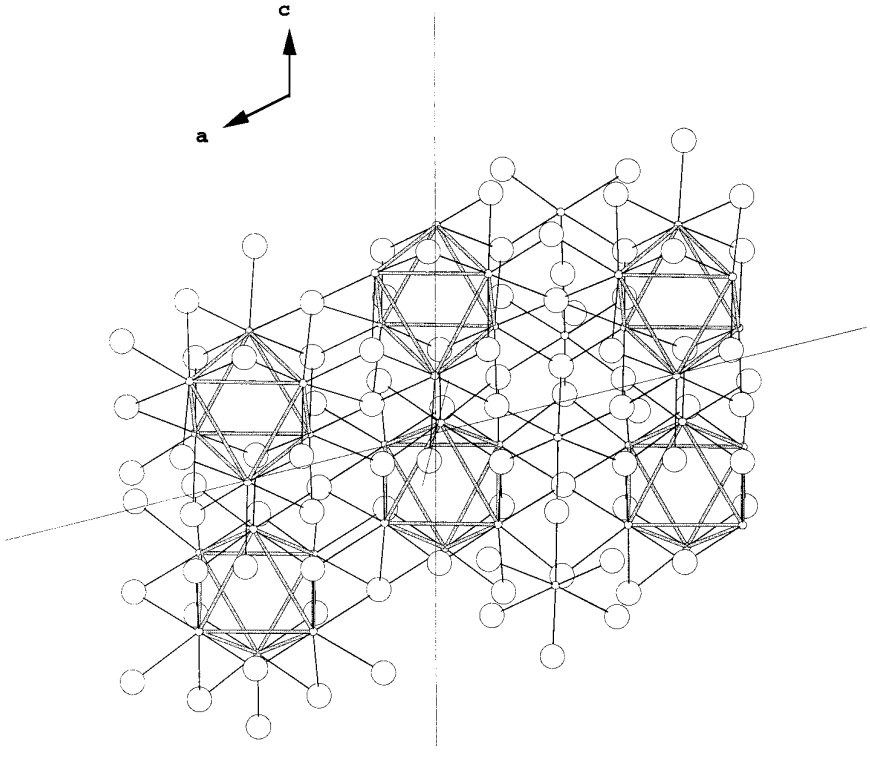

FIG. 3. Projection of $LaNb_7O_{12}$ on *ac* plane. Large open circles, O; small circles, Nb.

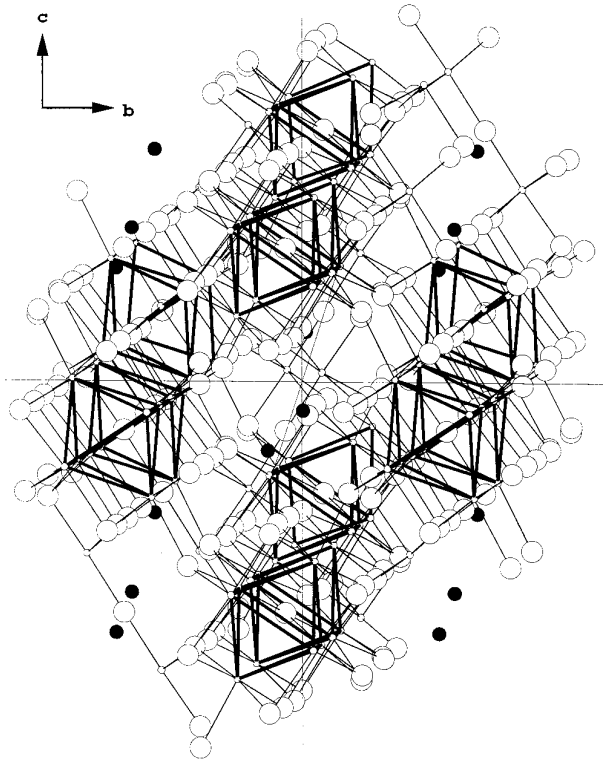

FIG. 4. Projection of $LaNb_7O_{12}$ on *bc* plane. Dark filled circles, La.

TABLE 6
Madelung Lattice Energy Values (Kcal/mol) for $LaNb_7O_{12}$[a]

La	1101.4 × 1	1101.4
Nb1	794.9 × 1	794.9
Nb2	779.8 × 1	779.8
Nb3	726.9 × 1	726.9
Nb4	723.5 × 1	723.5
Nb5	725.8 × 1	725.8
NB6	808.4 × 1	808.4
NB7	3074.3 × 1	3074.3
O1	478.3 × 1	478.3
O2	538.6 × 1	538.6
O3	460.0 × 1	460.0
O4	461.0 × 1	461.0
O5	468.3 × 1	468.3
O6	547.3 × 1	547.3
O7	491.7 × 1	491.7
O8	512.3 × 0.5	256.2
O9	567.5 × 1	567.5
O10	615.8 × 0.5	307.9
O11	528.3 × 1	528.3
O12	542.7 × 1	542.7
O13	411.6 × 1	411.6
		Σ14794.4

[a] Calculated using the positional parameters of $LaNb_7O_{12}$.

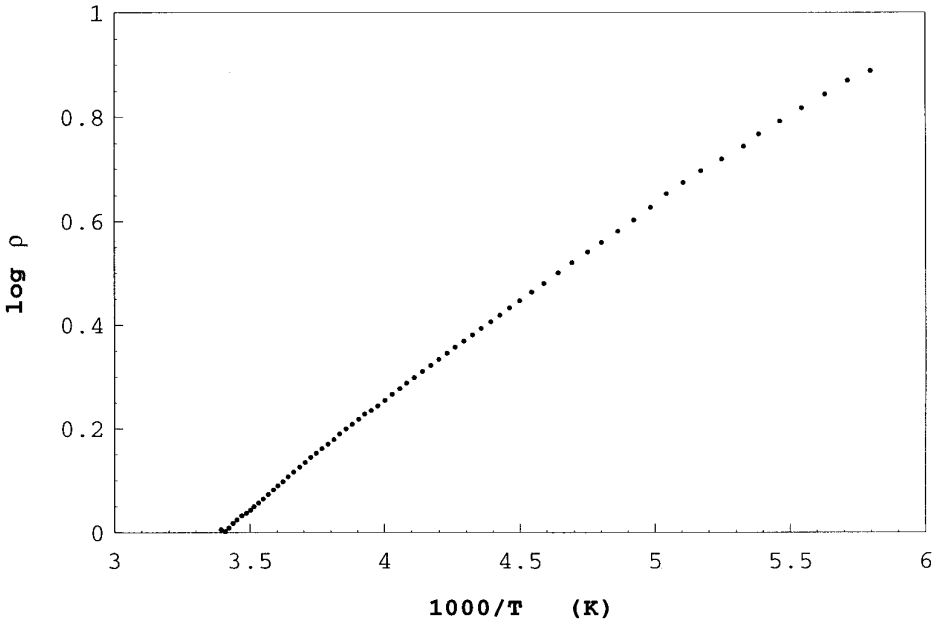

FIG. 5. Resistivity as a function of temperature of $LaNb_7O_{12}$.

MAPLE Values of $LaNb_7O_{12}$

It has been demonstrated in several niobium cluster compounds (9, 13, 15) that the concept of the Madelung part of the lattice energy (MAPLE) can be applied to oxides containing metal–metal bonds (16). The MAPLE value of $LaNb_7O_{12}$ from the positional parameters of the single crystal structure was calculated to be 14794.4 Kcal/mol (Table 6) (17). The sum of the MAPLE values for the hypothetical binary components according to Eq. [1] is

$$1/2\ La_2O_3 + 1/2\ Nb_2O_5 + \text{“}Nb_6O_8\text{”} = LaNb_7O_{12}$$
$$1/2(3387.7) + 1/2(9042.3) + 8615.5 = 14830.5\ \text{Kcal/mol}, \quad [1]$$

(where the value for the hypothetical binary oxide “Nb_6O_8” with 14 electrons in metal–metal bonding states was calculated from $Mg_3Nb_6O_{11}$ (13)) in excellent agreement (within 0.2% range) with the MAPLE value of $LaNb_7O_{12}$.

Electrical Resistivity and Magnetic Properties

Electrical resistivity measurements on a pressed pellet of $LaNb_7O_{12}$ reveal that the room temperature resistivity is ~98 $\Omega \cdot$ cm. The electrical resistivity as a function of temperature increases exponentially with decreasing temperature, indicating semiconducting behavior. The thermal activation energy (E_a) for conduction estimated from the linear portion of the plot of log ρ vs $1000/T$ (Fig. 5) in the temperature range 180–300 K is 0.08 (1) eV. Since the resistivity of the sample is relatively large, the small E_a reflects extrinsic effects and does not correspond to the band gap.

The molar susceptibility of $LaNb_7O_{12}$ as a function of temperature shown in Fig. 6 reveals that the susceptibility remains nearly temperature independent from room temperature to ~100 K and is weak, $\chi_{290} = 3.9 \times 10^{-5}$ emu/mol. A small peak at ~50 K probably arises from the antiferromagnetic ordering of absorbed O_2 (18). The upturn seen at low temperature suggests that magnetic impurities may be present in the sample.

Electronic Band Structure

In order to understand the electrical transport and magnetic properties of $LaNb_7O_{12}$ one turns to the electronic band structure. Although the electronic band diagram for $LaNb_7O_{12}$ has not be calculated, it is appropriate to use the band structure of $SrNb_8O_{14}$, which has similar structural units of Nb_6O_{12} discrete clusters and NbO_6 octahedra forming the network structure (13). Moreover, the Nb_6 octahedra in $SrNb_8O_{14}$ also have 14 electrons in Nb–Nb bands. Figure 7 shows the molecular orbital energy level diagram of the discrete $Nb_6O^i_{12}O^a_6$ unit (7a) and the band diagram of $SrNb_8O_{14}$ adopted for $LaNb_7O_{12}$ (7b). The left panel of Fig. 7 is derived from the molecular orbital level diagram of $Nb_6Cl^{4-}_{18}$ in which the a_{2u} is nonbonding (19). However, for the oxide cluster $Nb_6O^i_{12}O^a_6$, the a_{2u} level is dominated by antibonding character. Thus the gap between the a_{2u} and t_{2g} orbitals is significant. A group of seven orbitals (a_{1g}, t_{1u}, and t_{2g}) are bonding and filled

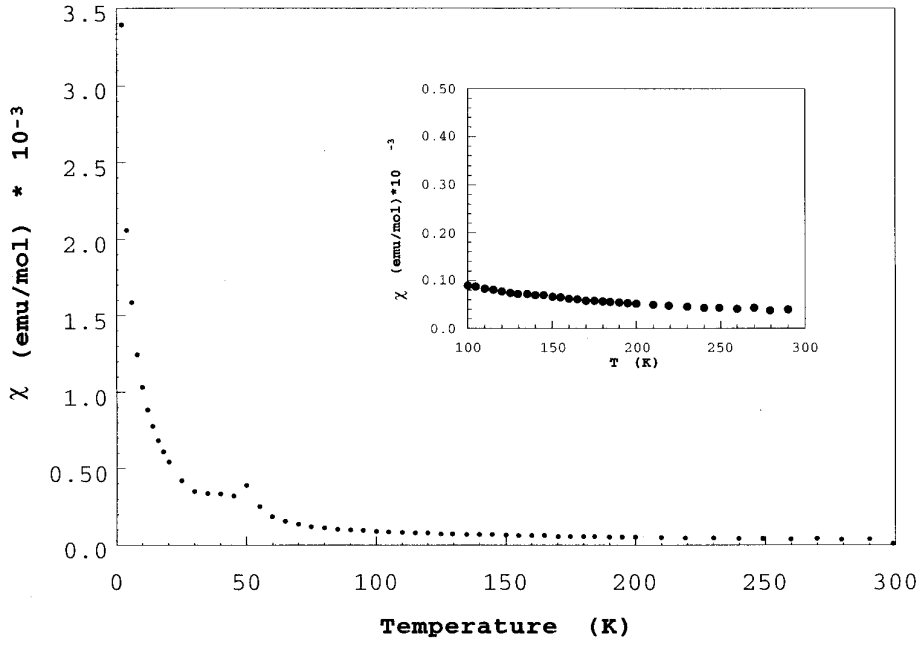

FIG. 6. Magnetic susceptibility as a function of temperature of $LaNb_7O_{12}$.

with 14 electrons while a_{2u} is antibonding and empty. In an extended lattice the discrete levels arising from this structure unit will broaden into bands (7b). It is clear that the M–M valence electrons fill up to the t_{2g} band and leave the a_{2g} band empty. This accounts for the semiconducting behavior. Since the Nb_6O_{12} clusters are not condensed, the bands (a_{1g}, t_{1u}, and t_{2g}) should be narrow. Furthermore, due to the distortion of Nb_6 octahedra, the degeneracy of the t_{2g} level may be removed, which would give rise to even narrower bands, as in $SrNb_8O_{14}$ (8). Electrons in filled narrow bands often show weak temperature-independent paramagnetism due to localization effects.

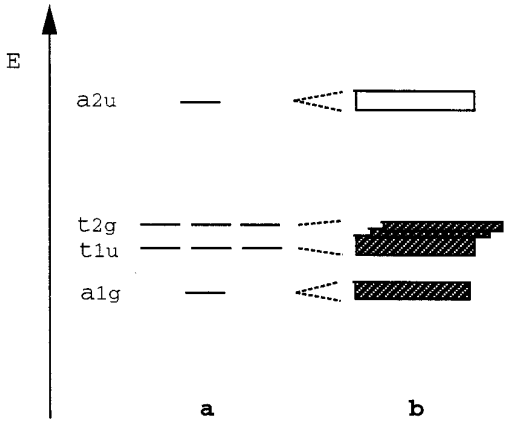

FIG. 7. A molecular orbital level for the Nb_6O_{18} cluster (a) and a possible resultant band scheme (b) for $LaNb_7O_{12}$.

The number of valence electrons in oxoniobates varies from 13 (9) to 15.5 (15). It is possible to replace lanthanum La^{3+} with divalent cations (A) in $LaNb_7O_{12}$, for example, alkaline earth metal cations, to change the valence electron count and the filling of the bands. To better understand how the physical properties of ANb_7O_{12} compounds vary with the number of valence electrons, we are currently in the process of preparing the analogous compounds with $A = Sr^{2+}$, Ba^{2+}, and Ca^{2+}.

CONCLUSION

$LaNb_7O_{12}$ is a new reduced oxoniobate containing discrete Nb_6O_{12} clusters with 14 valence electrons filling a set of narrow bands. It shows semiconducting behavior with a small $E_a \sim 0.08$ eV and weak temperature-independent paramagnetism. The small activation energy is attributed to extrinsic effects and does not correspond to the t_{2g}–a_{2u} energy gap.

ACKNOWLEDGMENTS

We thank Professor W. H. McCarroll for critically reading this manuscript and useful comments. Research was supported by the National Science Foundation Solid State Chemistry Grant DMR-93-14605.

REFERENCES

1. (a) J. D. Corbett and R. E. McCarley, *in* "Crystal Chemistry and Properties of Materials with Quasi-One-Dimensional Structures" (J. Rouxel, Ed.), p. 179. Reidel, Dordrecht, 1986; (b) R. Chevrel and

M. Sergent, *in* "Crystal Chemistry and Properties of Materials with Quasi-One-Dimensional Structures" (J. Rouxel, Ed.), p. 315. Reidel, Dordrecht, 1986.
2. B. Lindblom and R. Strandberg, *Acta Chem. Scand.* **43,** 825 (1989).
3. D. M. Evans and L. Katz, *J. Solid State Chem.* **6,** 459 (1973).
4. (a) B. O. Marinder, *Chem. Scr.* **11,** 97 (1977); (b) R. Burnus, J. Köhler, and A. Simon, *Z. Naturforsch.* **426,** 536 (1987).
5. J. Köhler and A. Simon, *Z. Anorg. Allg. Chem.* **553,** 106 (1987).
6. G. Svensson, J. Köhler, and A. Simon, *Angew. Chem. Int. Ed. Engl.* **31,** 212 (1992).
7. J. Köhler, A. Simon, R. Tischtau, and G. Miller, *Angew. Chem. Int. Ed. Engl.* **28,** 1662 (1989).
8. J. Köhler, G. Svensson, and A. Simon, *Angew. Chem. Int. Ed. Engl.* **31,** 1437 (1992).
9. J. Köhler, R. Tischtau, and A. Simon, *J. Chem. Soc. Dalton Trans.* 830 (1991).
10. L. H. Brixner, H.-Y. Chen, and C. M. Foris, *J. Solid State Chem.* **45,** 80 (1982).
11. J. C. Calabrese, L. H. Brixner, and C. M. Foris, *J. Solid State Chem.* **48,** 142 (1983).
12. I. D. Brown and D. Altermatt, *Acta Crystallogr. B* **41,** 244 (1985).
13. J. Köhler, A. Simon, J. Hibble, and A. K. Cheetham, *J. Less-Common Met.* **142,** 123 (1988).
14. J. Hibble, A. K. Cheetham, J. Köhler, and A. Simon, *J. Less-Common Met.* **154,** 271 (1989).
15. J. Köhler, R. Tischtau, and A. Simon, unpublished work.
16. R. Hoppe, *Angew. Chem. Int. Ed. Engl.* **5,** 95 (1966).
17. R. Hoppe, "MAPLE-Programm" zur Berechnung des Coulombanteils der Gitterenergie und partieller Madelungfaktoren, Giessen, 1977.
18. Quantum Design Technical Advisory MPMS No. 8, Quantum Design, Inc., 1990.
19. T. Hughbanks, *Prog. Solid State Chem.* **9,** 329 (1989).